Coordination Chemistry of the Pseudochalcogen Nitrite Analog Nitrosodicyanomethanide

D. Scott Bohle,*,† Brenda J. Conklin,‡ and Chen-Hsiung Hung†

Department of Chemistry, University of Wyoming, Laramie, Wyoming 82071-3838, and Department of Chemistry and Biochemistry, University of Colorado at Boulder, Boulder, Colorado 80309-0215

Received October 13, 1994[⊗]

Two complexes of the pseudohalide nitrosodicyanomethanide, $[ONC(CN)_2]^-$, with $Fe^{III}(TTP)[ONC(CN)_2]$, **1**, and $Ir^{I}[ONC(CN)_2](CO)(PPh_3)_2$, **2**, have been prepared and characterized by single-crystal X-ray crystallography, elemental analysis, electrochemistry, and IR, NMR, UV–vis, and ESR spectroscopy. This pair of complexes illustrates the ambidentate nature of the nitrosodicyanomethanide ligand. *Ab initio* calculations with Gaussian92 are used to rationalize the observed oxygen binding to iron in **1** and nitrogen binding to the iridium in **2**. The single-crystal X-ray diffraction results include the following: **1**, triclinic space group $P\bar{1}$, $a = 11.725(2)$ Å, $b = 13.851(3)$ Å, $c = 14.382(3)$ Å, $\alpha = 108.74(3)°$, $\beta = 95.07(3)°$, $\gamma = 108.19(3)°$, $Z = 2$; **2**, triclinic space group $P\bar{1}$, $a = 12.662(3)$ Å, $b = 13.896(3)$ Å, $c = 21.879(4)$ Å, $\alpha = 74.69(3)°$, $\beta = 78.65(3)°$, $\gamma = 83.10(3)°$, $Z = 4$.

Although the chemical similarities of anions such as halides, cyanide, thiocyanate, and azide are well recognized and embodied in the pseudohalide concept,[1] only a handful of reports have attempted to extend this principle to the derivatives of the group 16 elements, the pseudochalcogenides.[2] This difference is surprising as the initial outline of this concept was first described by Langmuir in his isosteric principle as early as 1919.[3] Examples of such species are the series $[NCN]^{2-}$, $[C(CN)_2]^{2-}$, and $[NNC]^{2-}$, which are pseudochalcogen analogues of O^{2-}, and the known anions $[O_2NNCN]^-$,[4] and $[O_2NC(CN)_2]^-$,[5] as well as the yet unreported anion $[O_2NCNN]^-$, which are pseudochalcogen analogues of nitrate. Although aspects of the theoretical basis for these relationships have been briefly explored,[6–8] there remain many gaps in our understanding of both the utility and limits of the principle. This is especially true for the pseudochalcogen analogs of the nitrite anion, for which only one, nitrosodicyanomethanide, $[ONC(CN)_2]^-$, is known and characterized.[9,10] As part of our research into the remarkable chemistry of nitrite complexes of iron porphyrins, we have prepared and characterized the first examples of coordinatively unsaturated nitrosodicyanomethanide transition metal complexes. In this paper we describe (1) the syntheses and structures of $Fe(TTP)\{\eta^1\text{-}ONC(CN)_2\}$, **1**, and $Ir\{\eta^1\text{-}N(O)C(CN)_2\}(CO)(PPh_3)_2$, **2**, (2) the first electrochemical characterization of this anion and its complexes with cyclic voltammetry, spectroelectrochemistry, and square-wave voltammetry, and (3) the first *ab initio* SCF calculations of the nitrosodicyanomethanide anion at the Hartree–Fock and second-order Møller–Plesset level of theory. Together these results provide insights into the coordination sphere reactivity of a nitrite anion analog that are relevant to understanding enzymatic nitrite reduction by certain anaerobic bacteria.

Results

Syntheses. The available silver and alkali metal salts of nitrosodicyanomethanide are only soluble in polar organic solvents such as ethanol, methanol, or acetonitrile.[9,11] In order to increase the range of possible solvents for this chemistry we have developed a synthesis of tetramethylammonium nitrosodicyanomethanide, **3**, by the metathesis reaction shown in eq 1.

$$Ag[ONC(CN)_2] + [NMe_4]Cl \longrightarrow [NMe_4][ONC(CN)_2] + AgCl \quad (1)$$
3

$$Fe(TTP)Cl + Ag[ONC(CN)_2] \longrightarrow Fe(TTP)[\eta^1\text{-}O\text{-}NC(CN)_2] + AgCl \quad (2)$$
1

$$[NMe_4][ONC(CN)_2] + IrCl(CO)(PPh_3)_2 \xrightarrow[-NMe_4Cl]{} Ir\{\eta^1\text{-}N(O)C(CN)_2\}(CO)(PPh_3)_2 \quad (3)$$
2

This new salt is isolated as bright yellow crystals, and its high solubility in acetonitrile and dichloromethane has allowed for its characterization by nonaqueous electrochemistry. The iron(III) porphyrin complex **1** is prepared by metathesis with $Ag[ONC(CN)_2]$, eq 2. The labile chloride in Vaska's complex is readily substituted either by direct metathesis with **3** to give $Ir\{\eta^1\text{-}N(O)C(CN)_2\}(CO)(PPh_3)_2$, **2**, eq 3, or by halide abstraction with $Ag[ONC(CN)_2]$. In general, nitrosodicyanomethanide salts and complexes are moderately hydrolytically sensitive and are handled in dry solvents under inert conditions.

† University of Wyoming.
‡ University of Colorado at Boulder.
⊗ Abstract published in *Advance ACS Abstracts,* April 1, 1995.

(1) Golub, A. M.; Köhler, H.; Skopenko, V. V. *Chemistry of Pseudohalides*; Clark, R. J. H., Ed.; Topics in Inorganic and General Chemistry, Monograph 21; Elsevier: Amsterdam, 1986.
(2) For reviews see: (a) Jäger, L.; Köhler, H. *Sulfur Rep.* **1992**, *12*, 159. (b) Köhler, H. *Nova Acta Leopold.* **1985**, *59*, 259.
(3) (a) Langmuir, I. *J. Am. Chem. Soc.* **1919**, *41*, 1543. (b) Langmuir, I. *J. Am. Chem. Soc.* **1920**, *42*, 274. (c) Langmuir, I. *Science* **1921**, *54*, 59.
(4) Harris, S. R. *J. Am. Chem. Soc.* **1958**, *80*, 2302.
(5) Köhler, H.; Eichler, B.; Kolbe, A. *Z. Chem.* **1969**, *10*, 154.
(6) Jäger, L.; Schädler, H.-D.; Grobe, U.; Köhler, H.; Nefedov, V. I. *Z. Anorg. Allg. Chem.* **1992**, *617*, 123.
(7) (a) Schädler, H.-D.; Jäger, L.; Senf, I. *Z. Anorg. Allg. Chem.* **1993**, *619*, 1115. (b) Schädler, H.-D.; Köhler, H. *Z. Chem.* **1990**, *30*, 67.
(8) Jensen, H.; Klewe, B.; Tjelta, E. *Acta Chem. Scand.* **1977**, *31A*, 151.
(9) Köhler, H.; Lux, G. *Inorg. Nucl. Chem. Lett.* **1968**, *4*, 133.
(10) Longo, G. *Gazz. Chim. Ital.* **1931**, *61*, 575.
(11) Iglesias, E.; Williams, D. L. H. *J. Chem. Soc., Perkin Trans. 2* **1989**, 343.

0020-1669/95/1334-2569$09.00/0

Table 1. Selected Metrical Parameters for **1**

		Bond Lengths (Å)			
		At the Iron and the Nitrosodicyanomethanide Ligand			
Fe(1)−N(3)	2.035(3)	Fe(1)−N(4)	2.038(4)	Fe(1)−N(2)	2.032(4)
Fe(1)−N(1)	2.040(4)	Fe(1)−O(1)	1.945(4)	O(1)−N(5)	1.330(5)
N(5)−C(49)	1.300(8)	C(51)−C(49)	1.420(9)	C(51)−N(7)	1.136(10)
C(50)−C(49)	1.440(8)	C(50)−N(6)	1.119(8)		
		Within the Porphyrin Ring			
N(1)−C(1)	1.393(5)	N(1)−C(4)	1.395(7)	C(1)−C(2)	1.423(6)
C(1)−C(41)	1.386(7)	C(3)−C(2)	1.327(8)	C(4)−C(3)	1.433(6)
C(4)−C(5)	1.378(7)	C(13)−C(5)	1.409(6)	N(2)−C(16)	1.378(5)
N(2)−C(13)	1.380(6)	C(13)−C(14)	1.428(7)	C(15)−C(14)	1.343(7)
C(16)−C(15)	1.448(7)	C(16)−C(17)	1.382(7)	C(25)−C(17)	1.412(7)
N(3)−C(28)	1.383(6)	N(3)−C(25)	1.387(5)	C(26)−C(27)	1.341(7)
C(25)−C(26)	1.408(7)	C(28)−C(29)	1.390(7)	C(28)−C(27)	1.436(7)
C(37)−C(29)	1.409(6)	N(4)−C(37)	1.393(6)	N(4)−C(40)	1.379(5)
C(37)−C(38)	1.419(7)	C(38)−C(39)	1.342(7)	C(40)−C(39)	1.426(7)
C(40)−C(41)	1.405(6)				
		Bond Angles (deg)			
		At the Iron and the Nitrosodicyanomethanide Ligand			
Fe(1)−O(1)−N(5)	114.6(3)	O(1)−N(5)−C(49)	113.6(5)	N(5)−C(49)−C(51)	124.5(5)
N(5)−C(49)−C(50)	116.0(6)	C(51)−C(49)−C(50)	119.5(6)	N(6)−C(50)−C(49)	178.8(5)
N(7)−C(51)−C(49)	179.3(5)	N(1)−Fe(1)−O(1)	101.5(1)	N(2)−Fe(1)−O(1)	100.9(2)
N(3)−Fe(1)−O(1)	96.4(2)	N(4)−Fe(1)−O(1)	102.0(2)	N(3)−Fe(1)−N(2)	88.6(1)
N(3)−Fe(1)−N(4)	88.3(1)	N(2)−Fe(1)−N(4)	157.2(2)	N(3)−Fe(1)−N(1)	162.2(2)
N(2)−Fe(1)−N(1)	88.3(1)	N(4)−Fe(1)−N(1)	87.8(2)		
		Within the Porphyrin Ring			
Fe(1)−N(1)−C(4)	124.4(3)	Fe(1)−N(1)−C(1)	126.6(3)	C(4)−N(1)−C(1)	105.5(3)
N(1)−C(4)−C(3)	108.6(4)	N(1)−C(4)−C(5)	125.0(4)	N(1)−C(1)−C(2)	109.3(4)
N(1)−C(1)−C(41)	124.3(4)	C(2)−C(1)−C(41)	126.4(4)	C(4)−C(3)−C(2)	108.3(4)
C(1)−C(2)−C(3)	108.1(4)	C(3)−C(4)−C(5)	126.4(5)	C(4)−C(5)−C(13)	124.7(5)
C(4)−C(5)−C(6)	118.3(4)	C(13)−C(5)−C(6)	117.0(4)	N(2)−C(16)−C(15)	109.0(4)
N(2)−C(13)−C(14)	110.0(4)	N(2)−C(13)−C(5)	124.5(4)	C(14)−C(13)−C(5)	125.5(5)
C(13)−C(14)−C(15)	107.3(5)	C(16)−C(15)−C(14)	107.4(4)	Fe(1)−N(2)−C(16)	126.5(3)
Fe(1)−N(2)−C(13)	127.2(2)	C(16)−N(2)−C(13)	106.0(4)	N(2)−C(16)−C(17)	126.0(4)
C(15)−C(16)−C(17)	124.8(4)	Fe(1)−N(3)−C(25)	124.2(3)	Fe(1)−N(3)−C(28)	124.6(2)
C(25)−N(3)−C(28)	105.7(4)	N(3)−C(25)−C(26)	109.6(4)	N(3)−C(25)−C(17)	124.1(4)
C(26)−C(25)−C(17)	126.2(4)	N(3)−C(28)−C(27)	109.1(4)	N(3)−C(28)−C(29)	124.9(4)
C(27)−C(28)−C(29)	125.9(5)	C(25)−C(26)−C(27)	108.4(4)	C(28)−C(27)−C(26)	107.1(5)
C(25)−C(17)−C(16)	123.9(4)	C(25)−C(17)−C(18)	116.4(4)	C(16)−C(17)−C(18)	119.6(4)
Fe(1)−N(4)−C(37)	127.5(3)	Fe(1)−N(4)−C(40)	127.6(3)	C(37)−N(4)−C(40)	104.9(4)
N(4)−C(37)−C(29)	124.0(4)	N(4)−C(37)−C(38)	109.9(4)	C(29)−C(37)−C(38)	126.0(4)
N(4)−C(40)−C(41)	125.4(5)	N(4)−C(40)−C(39)	110.1(4)	C(41)−C(40)−C(39)	124.4(4)
C(28)−C(29)−C(30)	118.7(4)	C(28)−C(29)−C(37)	124.5(4)	C(30)−C(29)−C(37)	116.8(4)
C(37)−C(38)−C(39)	107.5(5)	C(1)−C(41)−C(40)	124.3(4)	C(1)−C(41)−C(42)	118.3(4)
C(40)−C(41)−C(42)	117.4(5)	C(40)−C(39)−C(38)	107.4(4)		

Structural Studies. Compounds **1** and **2** have been characterized by single-crystal X-ray diffraction; selected metrical data and atomic positions for these two compounds are collected in Tables 1−4. Together these two structures illustrate the ambidentate nature of nitrosodicyanomethanide, which exhibits linkage isomerization similar to the nitrite ligand.

As depicted in Figure 1 nitrosodicyanomethanide is O-bound to a five-coordinate iron chelated in a saddle-shaped porphyrin in **1**. The atomic displacements from the mean C,N plane of the iron porphyrin unit in **1** are shown in Figure 2 and illustrate that the pyrrole β carbons are alternatively pairwise displaced about 0.5 Å above and below the plane of the porphyrin. There are no close contacts between the nitrosodicyanomethanide ligand and adjacent molecules, and the plane defined by this ligand bisects the N(1)−Fe(1)−N(2) bond angle with angles of 47.1 and 43.3°. An important reason that there are no extra ligand−iron contacts is the formation of a close π-stacked pair, Figure 3, related by inversion symmetry. The closest contacts between the pairs are 3.52 Å {N(3)−C(14)} and 3.62 Å {N(3)−C(15)}, with a mean plane separation of 3.84 Å. A 3.81 Å lateral shift in the iron of each dimer pair results in iron−iron and centroid−centroid separations of 5.836 and 5.315 Å, respectively. This geometry juxtaposes the iron directly above the center of a pyrrole ring of the stacked pair which protrudes into the saddle. These values that are typical of a type of observed π-interaction termed intermediate (group I) by Scheidt.[12] Other iron porphyrin complexes in this class are Fe(OEP)X, X = NCS, CS, and $OClO_3$. The saddle distortion in **1** is characterized by average displacements of the methine and pyrrole β carbons by 0.04 and 0.47 Å, respectively, from the mean plane of the porphyrin and by dihedral angles between the tolyl group and this plane of 67.0, 59.8, 54.1, and 83.8°. In comparison with that of other saddle-shaped iron(III) tetraarylporphyrins, this distortion is quite pronounced, with the pyrrole β center displaced about twice that typically found.[12] Finally, the iron is displaced 0.359 Å from the plane defined by the four nitrogen atoms and 0.35 Å from the best plane defined by the whole porphyrin ring.

By contrast, the nitrosodicyanomethanide complex in **2** is nitrogen bound and the crystal structure has two independent molecules of $Ir\{\eta^1\text{-}N(O)C(CN)_2\}(CO)(PPh_3)_2$ in the unit cell. As depicted in Figure 4 for one of the independent molecules, molecule A, nitrosodicyanomethanide is bound *trans* to the carbonyl in a square planar geometry typical of Vaska's type

(12) Scheidt, W. R.; Lee, Y. J. *Struct. Bonding* **1987**, *64*, 1.

Table 2. Selected Atomic Coordinates ($\times 10^4$) and Equivalent Isotropic Displacement Coefficients ($Å^2 \times 10^3$) for **1**

	x	*y*	*z*	*U*(eq)[a]
Fe(1)	964(1)	232(1)	2033(1)	37(1)
N(1)	2018(3)	1806(3)	2272(3)	40(2)
N(2)	1303(3)	−208(3)	626(3)	38(2)
N(3)	−476(3)	−1214(3)	1575(3)	40(2)
N(4)	140(3)	839(3)	3155(3)	34(2)
N(5)	3214(4)	44(3)	2497(3)	48(2)
N(6)	6144(5)	261(5)	2635(4)	85(3)
N(7)	3486(5)	−1023(5)	4341(4)	82(3)
O(1)	2104(3)	−211(3)	2712(2)	47(2)
C(1)	2253(4)	2719(4)	3140(3)	36(2)
C(2)	3363(5)	3552(4)	3188(4)	51(2)
C(3)	3800(4)	3179(4)	2381(4)	50(2)
C(4)	2955(4)	2104(4)	1771(3)	43(2)
C(5)	3023(4)	1472(4)	832(3)	41(2)
C(13)	2183(4)	410(4)	261(3)	42(2)
C(14)	2134(5)	−198(4)	−763(4)	50(3)
C(15)	1275(5)	−1196(4)	−1009(3)	49(2)
C(16)	782(4)	−1227(4)	−127(3)	41(2)
C(17)	−12(4)	−2155(4)	−40(3)	40(2)
C(25)	−553(4)	−2154(4)	799(3)	38(2)
C(26)	−1283(5)	−3080(4)	964(4)	52(2)
C(27)	−1689(5)	−2741(4)	1809(3)	52(2)
C(28)	−1206(4)	−1567(4)	2193(3)	38(2)
C(29)	−1458(4)	−887(4)	3029(3)	39(2)
C(37)	−870(4)	259(4)	3449(3)	38(2)
C(38)	−1186(4)	988(4)	4236(4)	47(2)
C(39)	−355(4)	1994(4)	4465(4)	50(2)
C(40)	467(4)	1910(4)	3794(3)	41(2)
C(41)	1504(4)	2785(4)	3833(3)	42(2)
C(49)	3991(5)	−181(4)	3017(4)	46(2)
C(50)	5208(5)	75(5)	2811(4)	56(3)
C(51)	3714(5)	−643(5)	3756(4)	52(3)

[a] Equivalent isotropic *U* defined as one-third of the trace of the orthogonalized $\mathbf{U}_{ij}$ tensor.

Table 3. Selected Metrical Parameters for Ir{η^1-N(O)C(CN)$_2$}(CO)(PPh$_3$)$_2$, **2**

	bond lengths (Å)	
	molecule A	molecule B
Ir−N(1)	2.089(14)	2.060(12)
Ir−C(4)	1.819(19)	1.833(18)
Ir−P(1)	2.338(4)	2.323(5)
Ir−P(2)	2.333(4)	2.326(5)
N(1)−O(1)	1.262(16)	1.265(17)
N(1)−C(1)	1.320(23)	1.364(18)
C(1)−C(2)	1.446(29)	1.406(22)
C(1)−C(3)	1.443(24)	1.442(22)
C(2)−N(2)	1.155(31)	1.158(24)
C(3)−N(3)	1.116(25)	1.132(24)
C(4)−O(4)	1.146(24)	1.143(22)
	bond angles (deg)	
	molecule A	molecule B
N(1)−Ir−C(4)	178.1(6)	177.3(6)
N(1)−Ir−P(1)	90.2(3)	90.5(5)
C(4)−Ir−P(1)	91.0(5)	88.8(6)
N(1)−Ir−P(2)	89.6(3)	92.1(5)
C(4)−Ir−P(2)	89.1(5)	89.1(6)
P(1)−Ir−P(2)	176.1(1)	170.5(1)
Ir−N(1)−O(1)	119.2(11)	119.3(9)
Ir−N(1)−C(1)	120.7(10)	124.4(9)
O(1)−N(1)−C(1)	120.1(15)	116.3(11)
N(1)−C(1)−C(2)	120.6(14)	120.0(13)
N(1)−C(1)−C(3)	120.7(17)	116.4(12)
C(2)−C(1)−C(3)	118.6(17)	123.3(13)
C(1)−C(2)−N(2)	175.9(17)	178.3(16)
C(1)−C(3)−N(3)	172.9(26)	174.7(23)
Ir−C(4)−O(4)	177.4(15)	179.5(13)

complexes. The phenyl rings of the triphenylphosphine ligands are eclipsed, and the metal is slightly domed, being 0.052 and 0.072 Å out of the planes defined by the four metal-bound atoms in molecules A and B, respectively. In each case, the slight square pyramidal distortion moves the iridium toward the oxygen of the nitrosodicyanomethanide ligand, the plane of which is oriented orthogonally to the plane defined by the atoms bound to the iridium, the largest dihedral angles between the two planes being 92 and 93° in molecules A and B, respectively. The iridium−nitrogen bond lengths in **2**, 2.089(14) and 2.060(12) Å in molecules A and B, respectively, are at the long end of the range 2.022−2.068 Å found for other structurally characterized Ir(I) complexes contained in the Cambridge Crystallographic Data Base.[13]

Table 4. Selected Atomic Coordinates ($\times 10^4$) and Equivalent Isotropic Displacement Coefficients ($Å^2 \times 10^3$) for Ir{η^1-N(O)C(CN)$_2$}(CO)(PPh$_3$)$_2$, **2**

	x	*y*	*z*	*U*(eq)[a]
IrA	1446(1)	1771(1)	609(1)	38(1)
N(1A)	2568(10)	2109(10)	1091(5)	42(5)
O(1A)	3187(9)	1413(9)	1359(5)	60(5)
C(1A)	2649(13)	3042(13)	1104(7)	49(7)
C(2A)	3470(15)	3284(13)	1403(8)	57(7)
N(2A)	4151(16)	3513(15)	1606(9)	97(9)
C(3A)	1952(16)	3846(15)	795(9)	62(8)
N(3A)	1444(15)	4524(13)	592(9)	84(8)
C(4A)	436(12)	1503(14)	201(8)	53(7)
O(4A)	−202(10)	1373(11)	−69(6)	73(6)
P(1A)	2665(3)	2143(3)	−360(2)	39(1)
P(2A)	189(3)	1514(3)	1562(2)	39(1)
C(11A)	2078(12)	2984(11)	−1015(7)	45(4)
C(21A)	3197(11)	1075(10)	−686(7)	37(3)
C(31A)	3833(12)	2768(11)	−338(7)	42(4)
C(41A)	−1084(12)	2266(12)	1452(7)	46(4)
C(51A)	−226(13)	250(12)	1900(8)	51(4)
C(61A)	580(13)	1869(12)	2219(8)	48(4)
IrB	6583(1)	2081(1)	6476(1)	43(1)
N(1B)	8149(10)	1915(10)	6010(6)	48(5)
O(1B)	8773(9)	1197(9)	6255(6)	60(5)
C(1B)	8579(10)	2533(12)	5442(7)	43(6)
C(2B)	9639(16)	2319(13)	5143(8)	57(7)
N(2B)	10508(13)	2164(13)	4885(9)	77(8)
C(3B)	7858(14)	3327(15)	5148(8)	56(7)
N(3B)	7348(14)	4000(12)	4916(8)	76(7)
O(4B)	4326(12)	2221(12)	7177(7)	95(8)
C(4B)	5195(15)	2166(12)	6910(8)	55(7)
P(1B)	6001(3)	1184(3)	5861(2)	41(1)
P(2B)	7033(4)	3210(3)	6984(2)	51(2)
C(11B)	4717(13)	1765(12)	5620(7)	46(4)
C(21B)	5782(12)	−117(11)	6265(7)	41(4)
C(31B)	6918(12)	1140(11)	5105(7)	42(4)
C(41B)	5952(15)	4181(14)	7008(9)	63(5)
C(51B)	7294(13)	2667(12)	7791(8)	49(4)
C(61B)	8260(13)	3866(12)	6593(8)	51(4)

[a] Equivalent isotropic *U* defined as one-third of the trace of the orthogonalized $\mathbf{U}_{ij}$ tensor.

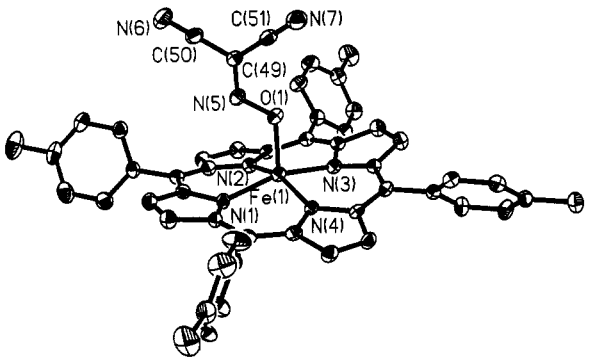

Figure 1. Full molecular structure of Fe(TTP){η^1-ONC(CN)$_2$}, **1**. In this and all subsequent ORTEP projections the hydrogen atoms have been omitted for clarity.

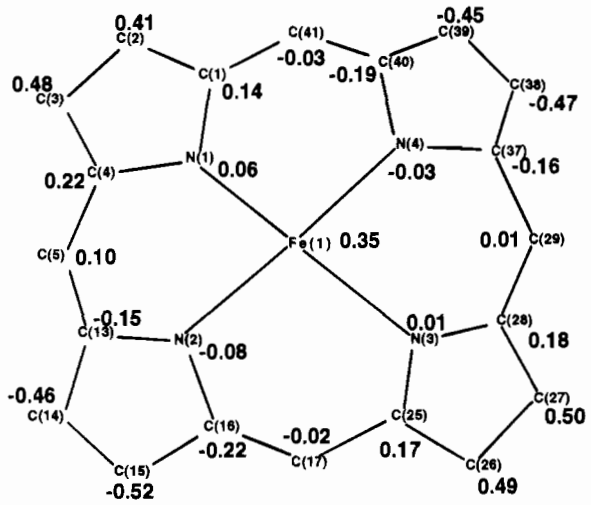

Figure 2. Out of plane displacements (Å) in **1**.

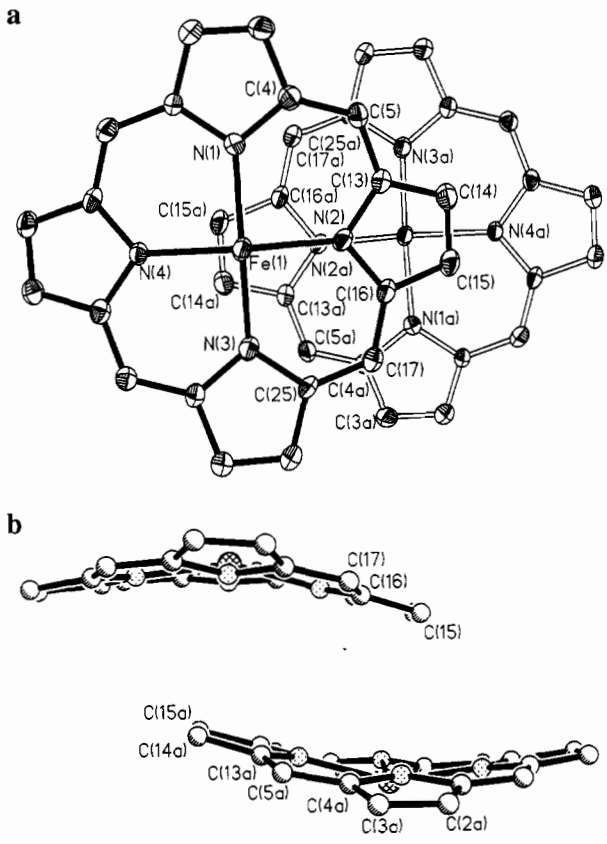

Figure 3. π-Stacking in the crystal structure of **1**: views normal to (a) and along (b) the mean plane defined by the porphyrin of the pair related by inversion symmetry. Closest intermolecular contacts are N(3)–C(14a), 3.52 Å, and 3.62 Å between N(4) and C(15a).

In Table 5 the crystallographic results for **1** and **2** are contrasted with literature and theoretically calculated values (see below). The most important trend present in these results is the difference in the effect binding via the oxygen or the nitrogen has on the nitrogen–oxygen and nitrogen–carbon bond lengths. Unfortunately, the high esd's, as well as their internal variance, associated with the dimensions of the lanthanide complexes, make these results difficult to rationalize. However, oxygen coordination leads to a lengthening of the N–O bond and

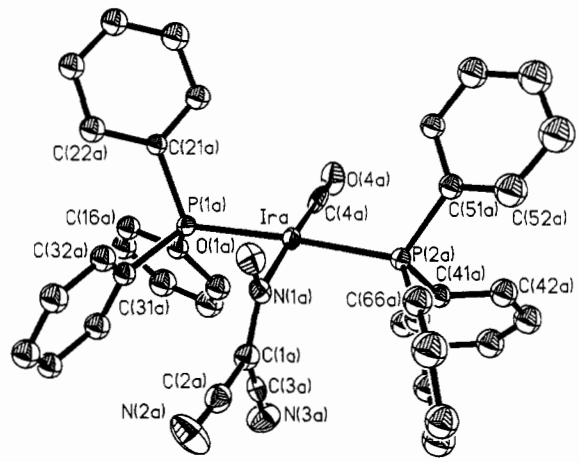

Figure 4. View of molecule A of Ir{η^1-N(O)C(CN)$_2$}(CO)(PPh$_3$)$_2$, **2**.

shortening of the C–N bond, suggesting that valence tautomer **A** contributes significantly to the binding. On the other hand,

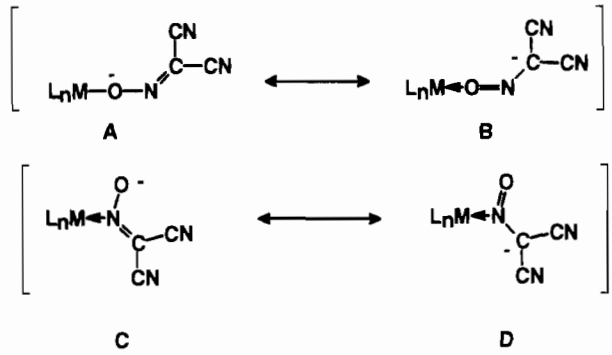

nitrogen coordination is best described by structure **D**, which has metrical parameters very similar to those calculated for the free ligand by *ab initio* techniques.

IR, UV–Vis, and ESR Spectroscopy. The infrared spectra of nitrosodicyanomethanide and its complexes have been discussed in detail;[15] selected data are collected for comparison in Table 5. General features of these spectra are the strong invariant cyanide stretching modes between 2250 and 2180 cm^{-1} and the coupling of the ν(NO) and ν(CC) modes in the backbone. Although assigning these bands for complex **2** and the tetramethylammonium salt **3** is straightforward, it was necessary to determine the difference IR spectrum, Figure 5, between **1** and Fe(TTP)Cl, in order to determine which bands of nitrosodicyanomethanide are overlapped by the porphyrin modes. In addition to the axial ligand bands indicated in Figure 5, several porphyrin bands at 1006, 811, and 727 cm^{-1}, marked with an asterisk in Figure 5, are also extremely sensitive to axial substitution. In general, it is difficult to assign the bands in these spectra because the tolyl and porphyrin ring modes are often extensively mixed.[16] The differences in the porphyrinic modes may also result from different porphyrin conformations. Although the structure of Fe(TTP)Cl is unknown, Fe(TPP)Cl has a domed C_{4h} geometry rather than the saddle conformation present in **1**.[17]

Possibly the most significant trend in these results is the difference, Δ, between the ν_s(CNO) and ν_s(CNO) modes for

(13) For example the iridium–nitrogen bond length in Ir{η^1-NCC(CN)$_2$}(CO)(PPh$_3$)$_2$ is 2.032 Å.[14]

(14) Wang, J.-C.; Shih, L. J.; Chen, Y.-J.; Wang, Y.; Fronczek, F. R.; Watkins, S. F. *Acta Crystallogr., Sect. B* **1993**, *49*, 680.

(15) Kolbe, A.; Köhler, H. *Z. Anorg. Allg. Chem.* **1970**, *373*, 230.

(16) Nakamoto, K. *Infrared and Raman Spectra of Inorganic and Coordination Compounds*, 4th ed.; Wiley-Interscience: New York, 1986; pp 213–21.

(17) Hoard, J. L.; Cohen, G. H.; Glick, M. D. *J. Am. Chem. Soc.* **1967**, *89*, 1992.

Table 5. Crystallographic, Theoretical, and Vibrational Data for Nitrosodicyanomethanide Complexes[a]

	r(N−O), Å	r(C−N), Å	∠(ONC), deg	ν(C≡N)	ν_a(CNO)	ν_s(CNO)	ref
			N-Bound				
Ir{η^1-N(O)C(CN)$_2$}(CO)(PPh$_3$)$_2$ (**3**)[b]	1.264(16)	1.342(21)	118.2(13)	2221, 2204	1377	1261	this work
Re{η^1-N(O)C(CN)$_2$}(CO)$_5$	1.26(1)	1.35(1)	117.0(8)	2221, 2207	1366	1311	29
			O-Bound				
Fe(TTP){η^1-ONC(CN)$_2$} (**2**)	1.330(5)	1.300(8)	113.6(5)	2232 (br)	1446	1240	this work
Yb{η^1-ONC(CN)$_2$}$_3${OP(NMe$_2$)$_3$}$_4$[c]	1.05(3)	1.55(4)	94(2)	*d*	*d*	*d*	45
	1.20(2)	1.37(3)	111(2)				
Nd{η^1-ONC(CN)$_2$}$_3${OP(NMe$_2$)$_3$}$_4$[c]	1.29(2)	1.28(4)	118(1)	*d*	*d*	*d*	46
	1.13(2)	1.59(4)	96(2)				
	1.28(2)	1.38(2)	114(2)				
			Other				
K{ONC(CN)$_2$} (ionic salt)	1.287(1)	1.324(2)	115.9(1)	*d*	*d*	*d*	47
Ag{η^2:μ_2-N(O)C(CN)$_2$} (mixed)	1.18	1.44	112	2246, 2232	1322	1289, 1270	48
			Theory[e]				
HF(3-21G)	1.2782	1.3383	116.74				this work
HF(6-31G*)	1.2184	1.3412	117.89				this work
HF(6-311G*)	1.2101	1.3414	118.17				this work
HF(6-311+G(2d,2p))	1.2138	1.3345	118.43				this work
MP2(6-31G*)	1.2771	1.3641	115.49	2206.8, 2181.0	1524.7	1387.9	this work
MP2(6-311G*)	1.2611	1.3652	116.03				this work
MP2(6-311+G(2d,2p))	1.2731	1.3541	116.15				this work

[a] Vibrational data given in cm^{-1} and measured in the solid state. [b] Average of the data for the two equivalent molecules in the structure of **2**. [c] Only two coordinated nitrosodicyanomethanide ligands reported; the third is in a disordered noncoordinated site. [d] Not reported. [e] Metrical data for optimized geometries for the *ab initio* method and basis set in parentheses. Note that frequency calculations were only performed at the MP2 level.

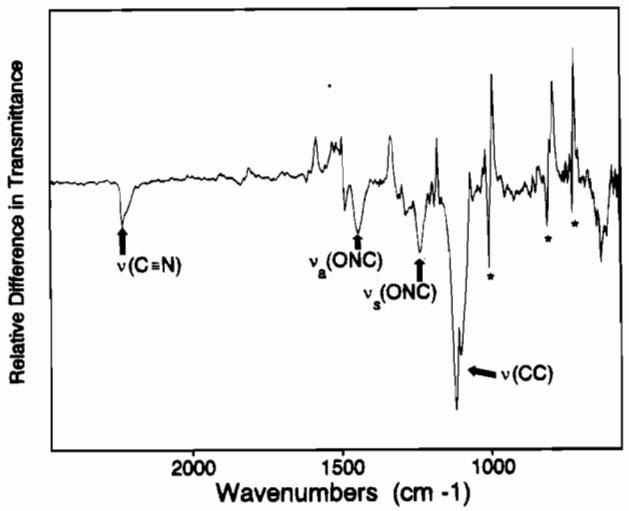

Figure 5. Difference infrared spectrum (KBr) of Fe(TTP){η^1-ONC(CN)$_2$}, **1**, and Fe(TTP)Cl, with the assigned modes due to the nitrosodicyanomethanide ligand indicated. Axial-ligand-sensitive modes of the porphyrin ligand are marked with an asterisk.

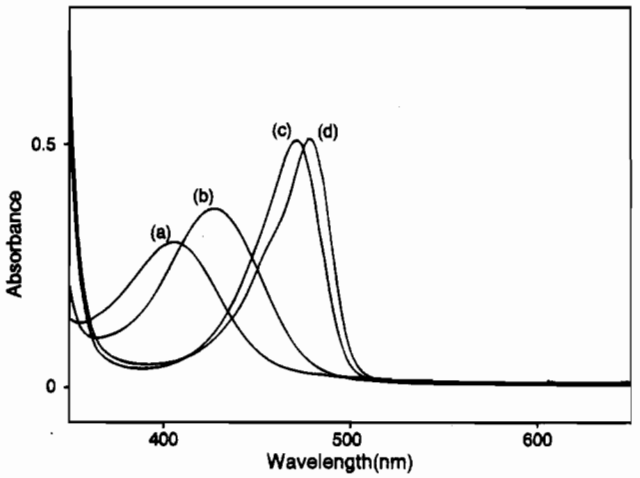

Figure 6. Solution UV−vis spectra of {NMe$_4$}[ONC(CN)$_2$], **3**: (a) in water, 406 nm; (b) in ethanol, 428 nm; (c) in acetonitrile, 472 nm; (d) in acetone, 478 nm.

the O *vs* the N bound complexes. For **1** Δ = 206 cm^{-1}, while for the N bound complexes the average of Δ is 86 cm^{-1}. These data are consistent with the trends observed for O-bound nitrite ligands (nitrito) where the ranges are ν(N=O) 1485−1400 cm^{-1} and ν(N−O) 1110−1050 cm^{-1}, Δ = 435−290 cm^{-1}. On the other hand, the N-bound nitrite ligands (nitro) have ranges for ν_s(NO$_2$) of 1470−1370 cm^{-1} and ν_s(NO$_2$) of 1340−1300 cm^{-1}, Δ = 170−30 cm^{-1}.[18] In the solid state **2** has a pronounced splitting of the carbonyl stretch by 25 cm^{-1}, which is due to the two distinctly different orientations of the molecules in the unit cell. In chloroform the ν(CO) mode for **2** is 1994 cm^{-1}, which is at the high end of the range, 1990−1949 cm^{-1}, for IrX(CO)(PPh$_3$)$_2$ compounds and is comparable to the cyano and −N=C=C(CN)$_2$ complexes.[19] UV−vis spectroscopic data for nitrosodicyanomethanide complexes are limited to a single report of the alkali metal salts in water which have λ_{max} (ϵ) values of 405 (80) and 286 (11 800) nm.[9] The greater solubility of the tetramethylammonium salt **3** allows for the measurement of solution spectra in a wider range of solvents. The spectra, shown in Figure 6, exhibit considerable solvatochromism. In the polar aprotic solvents acetone and acetonitrile the band is sharp and red-shifted by *ca.* 75 nm compared to that in protic solvents. This behavior, along with the small extinction coefficients, is consistent with the band being due to a n → π^* transition. In water and ethanol more intense high-energy bands are observed, λ_{max} (log ϵ) 266 nm (5.05) and 298 nm (3.89), respectively, which are most likely associated with a π → π^* transition. When the solvents are coordinated to either complex **1** or **2**, these bands are swamped by other transitions. Note though that the UV−vis spectrum for **1** is very similar to that of Fe(TTP)Cl in both the energy and intensity of the observed bands, with the exception that the Soret band is slightly blue-shifted by 4 nm for **1**.

In order to define the electronic structure of **1**, we have measured both its ESR spectrum and its magnetic susceptibility

(18) See ref 16, pp 221−7.
(19) (a) Vaska, L.; Jun, J. P. *J. Chem. Soc., Chem. Commun.* **1971**, 418. (b) Schlodder, R.; Vogler, S.; Beck, W. *Z. Naturforsch., B* **1972**, *27B*, 463.

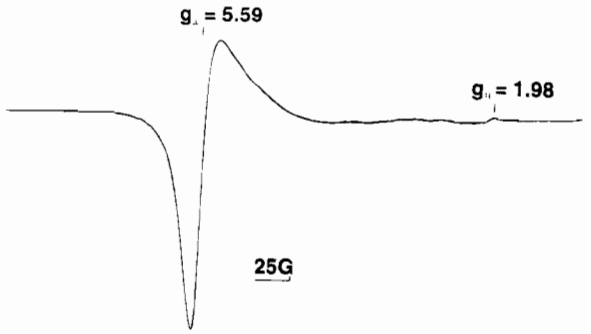

Figure 7. X-band ESR spectrum of **1** in a toluene glass at 77 K.

between 400 and 40 K. The ESR spectrum of **1** at 77 K, Figure 7, measured in a toluene glass, is a typical axial pattern with two peaks at $g_{\parallel} = 1.98$ and $g_{\perp} = 5.59$. These values are typical of high-spin iron(III) porphyrins in an axially symmetric environment. The variable-temperature SQUID magnetometric results for microcrystalline **1**, shown in Figure 8, are also consistent with **1** being a high spin $S = {}^5/_2$ complex. This system has a linear Currie plot, Figure 8 (inset), with constants $C = 3.56$ emu K mol^{-1} and $\Theta = -4$ K.

Electrochemistry. The only electrochemical datum available for the nitrosodicyanomethanide anion or its complexes is the polarographic reduction at -1.4 V of its potassium salt by a hanging mercury drop electrode at various pHs.[20] In water the reduction products are hydroxylamine and malononitrile, eq 4.

$$HONC(CN)_2 + 5H^+ + 4e^- \longrightarrow H_3NOH^+ + H_2C(CN)_2 \quad (4)$$

In DMF with 0.1 M [NEt_4]I as supporting electrolyte, two reductions are observed. On the other hand, cyclic voltammetric experiments on **3**, Figure 9 and Table 6, are dominated by an irreversible oxidation at 768 mV. Two product waves are also observed in these traces at -857 and -1160 mV. Under identical conditions, acetonitrile with 0.1 M TBAP supporting electrolyte, with a platinum electrode and a Ag/AgCl reference electrode tetramethylammonium nitrite has an irreversible oxidation at 998 mV, approximately 200 mV higher than that for **3**. The oxidative process has been followed by spectroelectrochemistry, and representative spectra, shown in Figure 10, illustrate that the initial absorbance at 472 nm is replaced by a new more intense band at 416 nm upon sweeping the potential through this irreversible process. Even at fast scan rates, up to 1000 mV s^{-1}, these spectra are not isosbestic and it is quite clear that other reaction(s) follow the initial oxidation. One possible reaction is that the one-electron oxidation of nitrosodicyanomethanide is followed by a rapid dimerization to a give the unknown azine dioxide **E**, [$(NC)_2CN(O)N(O)C(CN)_2$], eq 5. Although our data are consistent with the

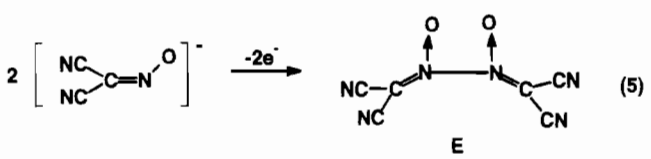

(5)

formation of **E** and a related dimerization of the [$R_2C{=}N{\rightarrow}O$] radical has been proposed,[21] there is surprisingly little information about azine dioxides.[22]

The cyclic voltammogram of **1**, Figure 11, is dominated by porphyrin- and metal-based processes and does not have bands that are directly attributable to the nitrosodicyanomethanide ligand. The Fe(III)/Fe(II) couple occurs at relatively low potentials, -825 mV with respect to ferrocene, and is also only quasireversible. This value is some 100 mV less than that for the closely related chloride complex Fe(TPP)Cl and comparable to the potentials for the azido complex.[23] Finally, the iridium nitrosodicyanomethanide complex **2** has only an irreversible reduction at -2144 mV as determined by cyclic voltammetry.

Theoretical Results. In order to determine the factors which control N vs O coordination in the complexes of nitrosodicyanomethanide, we have performed SCF *ab initio* calculations for the anion at both the Hartree–Fock and the Møller–Plesset levels of theory. The optimized ground state geometry calculated for a 6-311+G(2d,2p) basis set with the MP2 level of theory is shown in Figure 12; important figures from these calculations are collected in Tables 5 and 7. For comparison, a few representative theoretical results for the nitrite anion are also included in Table 7. A complete table of calculated interatomic distances and angles is included in the supplementary material (Table S12). The ground state geometry which corresponds to these structures is planar with C_s symmetry. Overall, increases in either the basis sets or the level of theory result in only slight changes in the structure and orbital energies: the N(1)–C(1) bond length increases slightly, and the energy of the HOMO decreases with increases in the basis set and level of the calculation. The largest difference between the HF and MP2 calculations for the 6-31G* basis set is the 2.4° decrease in the O–N(1)–C(1) bond angle. The charge distribution in these calculations are almost invariant, with Mulliken population analysis indicating that most of the negative charge resides on the two terminal nitrogens and the oxygen, while the nitroso nitrogen and C(1) are almost neutral. The frontier orbitals, not shown, reflect these trends. For example, for the 6-311G*/MP2 calculation both the HOMO and LUMO are π type orbitals with the next lowest and highest orbitals being σ orbitals with A′ symmetry. For the two highest occupied orbitals the electron density is highly polarized toward the oxygen, while the first and second virtual orbital, which are separated by only 0.050 eV, are localized primarily on N(1) and C(1). These results fit the observed binding patterns illustrated in Table 5 in that relatively high-oxidation-state metals prefer to bind nitrosodicyanomethanide through the oxygen, while electron-rich organometallic centers bind through the nitrogen.

The calculated frequencies and normal modes for nitrosodicyanomethanide are shown in Figure 13. Frequencies for both ^{14}N and ^{15}N (complete isotopic substitution) are listed under each mode. These values were determined for the optimized structure at the MP2/6-31G* level of theory. Due to the C_s symmetry of the anion, all modes are both IR and Raman active. The highest energy modes correspond to the stretches of the cyano groups in what is attributable to an asymmetric and symmetric manner, with the cyano group oriented *trans* to the nitroso group dominating the highest energy mode. The calculated bands assigned to the ν_a and ν_s modes, ν_3 and ν_4, are shifted by 28.7 and 15 cm^{-1}, respectively, trends which agree well with the experimentally reported values but whose absolute values are somewhat larger than those observed for the potassium salt by 14 and 10 cm^{-1}, respectively. With the exception of the ν_3 and ν_4 modes, the frequencies correspond

(20) Matschiner, H.; Köhler, H.; Matuschke, R. *Z. Anorg. Allg. Chem.* **1971**, *380*, 267.
(21) Horner, L.; Hockenberger, L.; Kirmse, W. *Chem. Ber.* **1961**, *94*, 290.
(22) For example see: *Methoden der Organischen Chemie (Houben-Weyl)*; Thieme: Stuttgart, Germany, 1967; Vol. 10, Part II, pp 121–2.
(23) Kadish, K. M. In *Iron Porphyrins, Part 2*; Lever, Gray, Eds.; Addison-Wesley: Reading, MA, 1983; p 161.

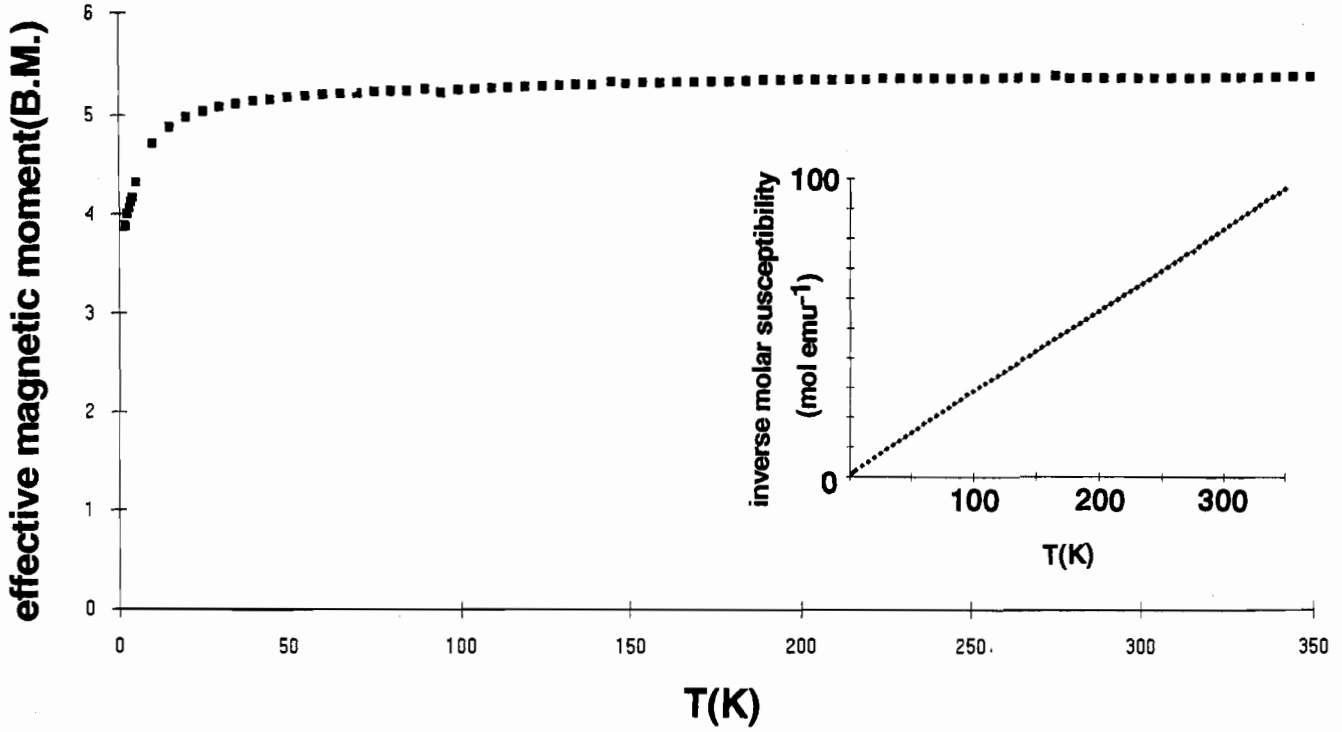

Figure 8. Variable-temperature magnetic susceptibility results for a microcrystalline sample of **1**. Inset shows a linear Curie plot which corresponds to $C = 3.56$ emu K mol^{-1} and $\Theta = -4$ K.

Table 6. Electrochemical Results[a]

compound	observed processes[b]		
Fe(TTP){ONC(CN)$_2$} (**1**)[c]	+638 r (FeTTP/FeTTP$^+$)	−825 ir (Fe^{II}/Fe^{III})	−1582 qr (FeTTP/FeTTP$^-$)
Ir{ONC(CN)$_2$}(CO)(PPh$_3$)$_2$ (**2**)[c]			−2144 ir (Ir^I/Ir^0)
[NMe$_4$][ONC(CN)$_2$] (**3**)[d]	+768 qr (ONC(CN)$_2^-$/ONC(CN)$_2$)	−852 ir (pw)	−1160 ir (pw)

[a] All values are in mV and are referenced to ferrocene and determined by square-wave voltammetry with the apparatus described in the Experimental Section. [b] Values of the potentials for the processes are followed by a description of the wave form in cyclic voltammetry and then the assignment in parentheses. Abbreviations: r = reversible, ir = irreversible, qr = quasireversible, pw = product wave. [c] Dichloromethane used as solvent. [d] Acetonitrile used as solvent.

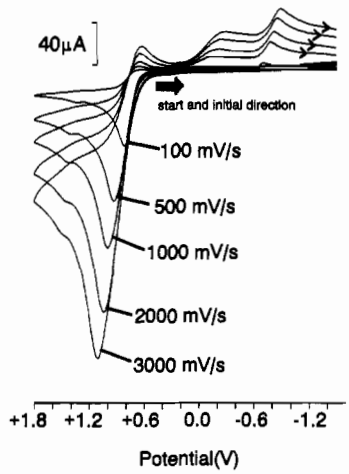

Figure 9. Cyclic voltammograms for {NMe$_4$}[ONC(CN)$_2$], **3**, with different sweep rates. All electrochemical experiments were measured in acetonitrile with 0.1 M TBAP as supporting electrolyte.

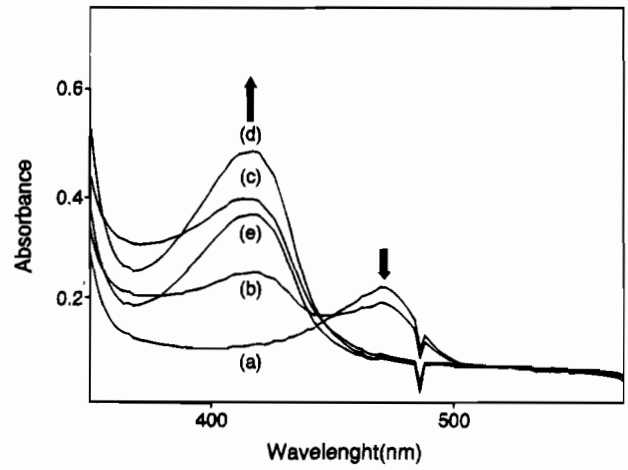

Figure 10. Spectroelectrochemical changes for the irreversible oxidation of **3** in acetonitrile showing the disappearance of the peak at 472 nm and the rise in the new peak at 416 nm. Scan rate was 10 mV s^{-1} with the following potentials (mV) [times (s)]: (a) 600 [0], (b) 1200 [60]; (c) 1500 [90]; (d) 1800 [120]; (e) 1800 [190].

closely to the observed values for the simple salts, with the closest match being between these modes for **1**, which contains an O-bound ligand; see Table 5. The differences between experiment and theory are not too surprising, given the delocalized nature of the bonding in this anion and the use of a limited basis set without polarized functions for the vibrational calculations. It is well-known that these functions are important for *ab initio* calculations of charged structures.[24] Nevertheless, these calculations lend considerable support to the recognition of the ambidentate nature of the nitrosodicyanomethanide ligand.

Reactions of Nitrosodicyanomethanide Complexes. At the outset of this research it was anticipated that nitrosodicy-

(24) Clark, T.; Chandrasekhar, J.; Spitznagel, G.; Schleyer, P. v. R. *J. Comput. Chem.* **1983**, *4*, 294.

Table 7. *Ab Initio* Results for Optimized Ground State Geometries of $[ONC(CN)_2]^-$ and NO_2^-

$[ONC(CN)_2]^-$

				total atomic charges[a]						
method and basis	total SCF energy (AU)	HOMO (eV)	LUMO (eV)[b]	O	N(1)	C(1)	C(2)	N(2)	C(3)	N(3)
HF 3-21G	−349.768464	−0.14851	0.28762	−0.53	−0.10	+0.16	+0.35	−0.60	+0.33	−0.61
HF 6-31G*	−351.762237	−0.15994	0.28626	−0.55	+0.02	0.00	+0.32	−0.54	+0.31	−0.55
HF 6-311G*	−351.846585	−0.16505	0.28029	−0.48	+0.02	−0.03	+0.18	−0.42	+0.17	−0.43
HF 6-311+G(2d,2p)	−351.871915	−0.17630	0.17901	*c*						
MP2 6-31G*	−351.746984	−0.16328	0.26080	−0.55	+0.01	+0.02	+0.34	−0.56	+0.32	−0.57
MP2 6-311G*	−351.832845	−0.16803	0.25673	−0.49	+0.01	0.00	+0.18	−0.43	+0.16	−0.44
MP2 6-311+G(2d,2p)	−351.858121	−0.18012	0.17820	*c*						

NO_2^-

				total atomic charges[a]		optimized geometry	
method and basis	total SCF energy (AU)	HOMO (eV)	LUMO (eV)[b]	O	N	N−O (Å)	O−N−O (deg)
HF 3-21G	−202.875309	−0.09943 (A1)	0.42028 (B1)	−0.63	+0.26	1.2865	116.39
HF 6-311G*	−204.122872	−0.12171	0.42760	−0.59	+0.17	1.2219	116.95
MP2 6-311G*	−204.116627	−0.13769	0.39821	−0.59	+0.19	1.2684	115.72

[a] Atomic numbering is as shown in Figure 9; determined by Mulliken population analysis. [b] Energy of first virtual orbital. [c] Not determined.

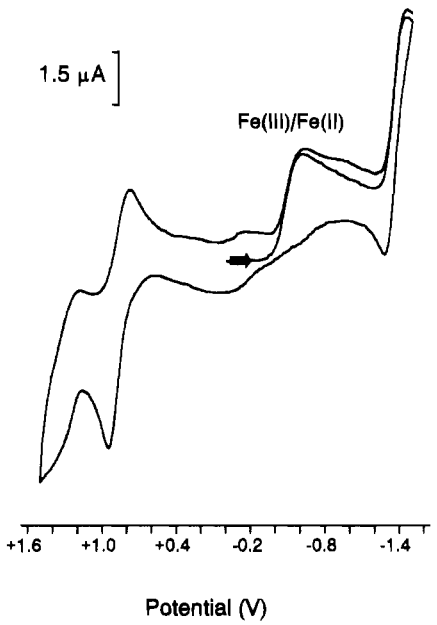

Figure 11. Cyclic voltammogram for Fe(TTP){η^1-ONC(CN)$_2$}, **1**, at 100 mV s^{-1} showing the quasireversible Fe(II)/Fe(III) couple at −825 mV with respect to Fc/Fc$^+$.

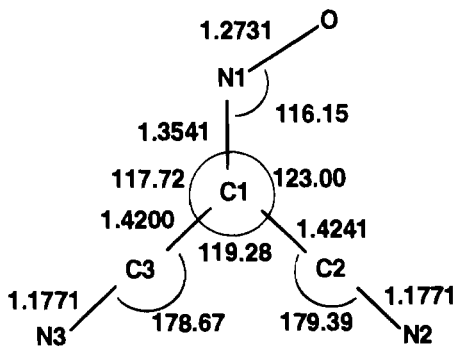

Figure 12. *Ab initio* optimized geometry of the nitrosodicyanomethanide anion calculated with Gaussian92 at the MP2/6311+G(2d,2p) level of theory. Bond lengths are in Å, and bond angles, in degrees.

anomethanide might share many reactions in common with nitrite ligands. In particular, we sought to determine if its complexes would transfer an oxygen or a dicyanomethanide to Lewis bases such as phosphines, thereby allowing new access to nitrosyl compounds or to novel species, **F**, with an {η^1-N=C-(CN)$_2$} ligand. Alternatively, it was anticipated that oxidative addition by low-valent metal centers via η^2-coordination as is shown in **G** might lead to the simultaneous introduction of a nitric oxide and dicyanocarbene ligand into the coordination sphere of the metal. To test the second possibility, complex **2** was thermolized in a variety of solvents under inert atmospheric conditions without any evidence for a reaction other than decomposition. For example, after reflux in toluene at 101 °C for 12 h, **2** is recovered in 78% return. There is no observed reaction between **1** and triphenylphosphine under the same conditions (ambient temperatures, 2 h, benzene) as have been found to yield nitrosyl complexes from Fe(TTP)(NO$_2$)py.[25]

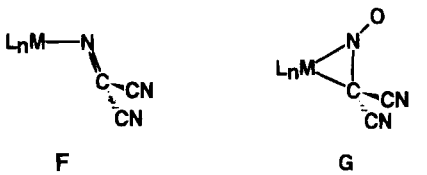

Kinetics and Thermodynamics of Ligand Binding to 1. In order to characterize the dynamics of ligand binding to **1**, we have measured spectrophotometric titrations and kinetics for the addition and substitution of pyridine to **1** to give [Fe(TTP)-(py)$_2$]$^+$ as the ultimate product. The reaction scheme used to interpret these results is shown in eqs 6 and 7 and involves the

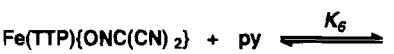

(6)

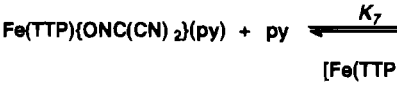

(7)

generation of a six-coordinate intermediate Fe(TTP)(py){η^1-ONC(CN)$_2$}, **H**. Figure 14 shows a plot for the spectrophotometric titration of **1** as a 1 × 10^{-4} M solution in toluene at 25 °C, with 525 μL aliquots of a 5 M pyridine solution in toluene, to give net pyridine concentrations in the range from 0 to 0.58

(25) Bohle, D. S.; Hung, C.-H. Unpublished results.

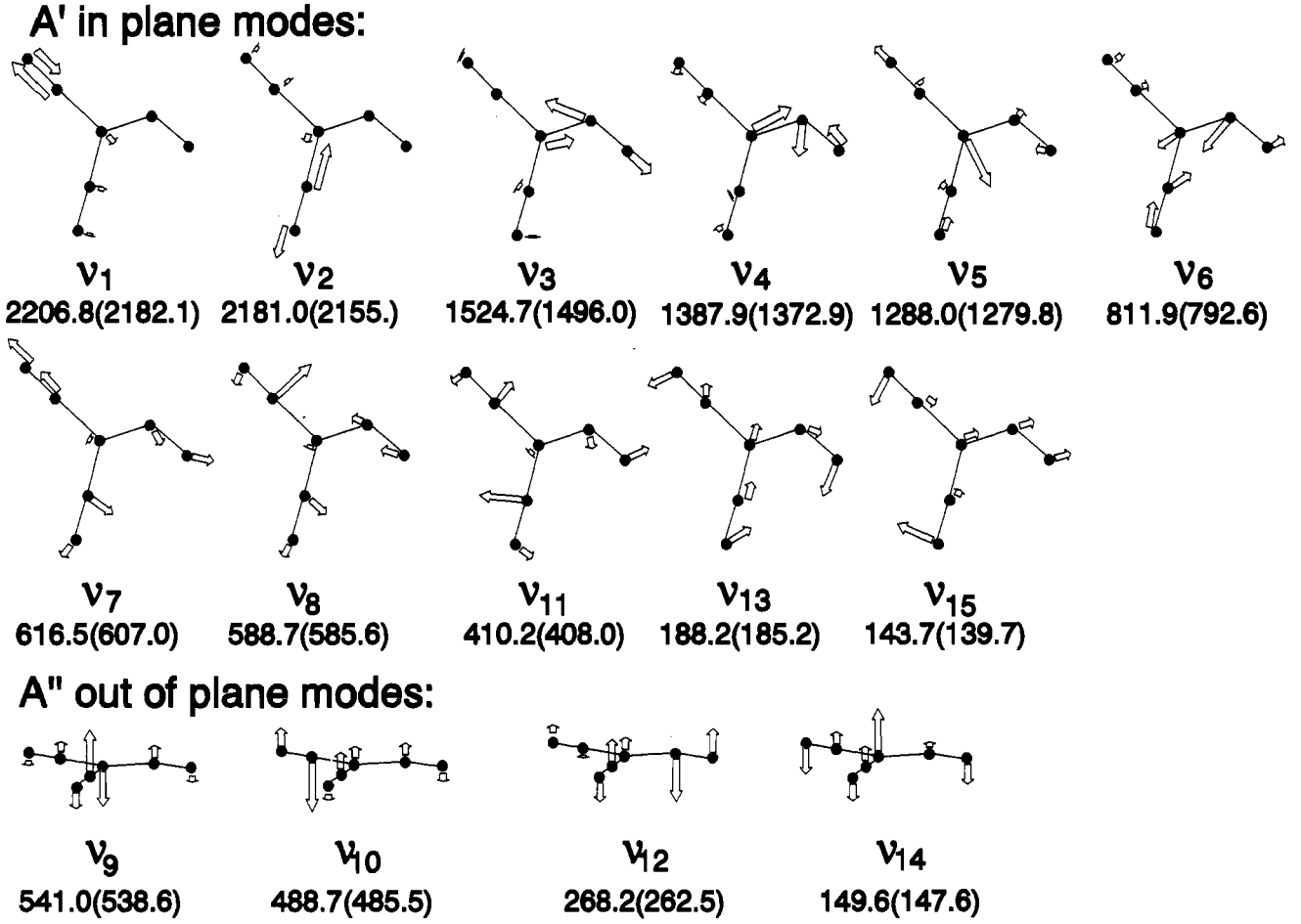

Figure 13. Calculated normal modes for the nitrosodicyanomethanide anion at the MP2/6-31G* level of theory. Frequencies are given in cm^{-1}, and values for the ^{15}N isotopically labeled product are listed in parentheses.

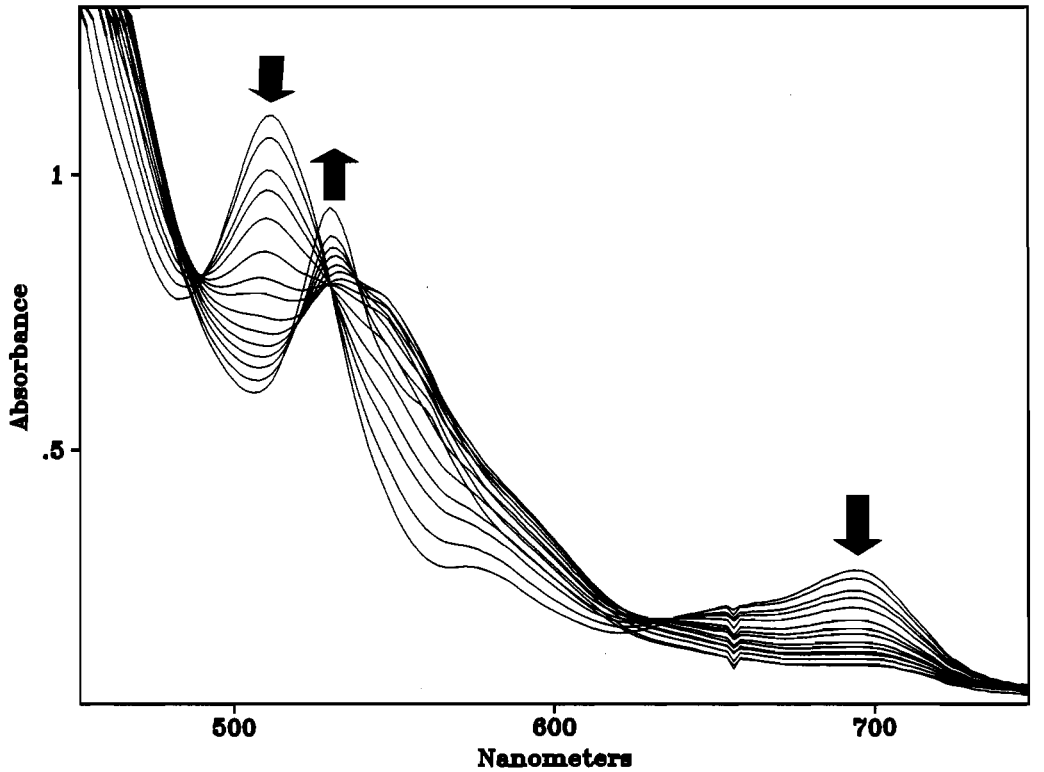

Figure 14. Spectrophotometric titration of **1** in a toluene with pyridine, showing contact regions 490−500, 530−550, and 620−640 nm.

M. The spectra have three main contact regions in the ranges 490−500, 530−550, and 620−640 nm, with the initial and final sets exhibiting an isosbestic-like set of points corresponding to eqs 6 and 7, respectively. Extracted absorbance data for three

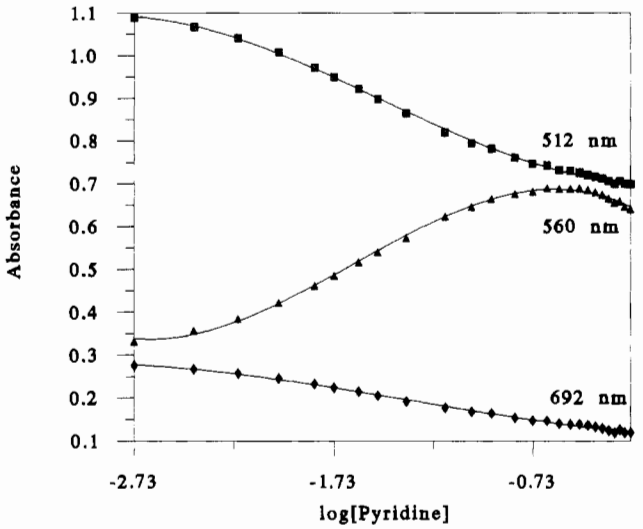

Figure 15. Extracted absorbance data from the titration in Figure 14 for three wavelengths with the largest net change.

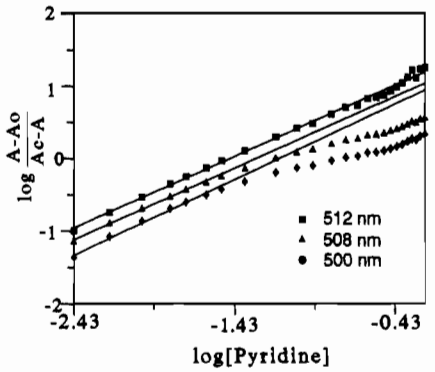

Figure 16. Double log plot for the initial additions of pyridine to **1** from the spectrophotometric titration of **1** in Figure 14. Best fit lines for the initial data are shown.

wavelengths are shown in Figure 15, where absorbance is plotted as a function of log([py]). These data are consistent with a titration according to eqs 6 and 7, as their A-diagrams (not shown) have the characteristic bell shape consistent with an equilibrium of three chromophoric species.[26] To determine the equilibrium constant for eq 6, we constructed log([py]) vs log-$[(A - A_0)/(A_c - A)]$ plots, Figure 16, according to the method of Walker, who described closely related studies for the base substitution with Fe(TPP)Cl.[27] In these cases the addition of nitrogen bases to Fe(TPP)Cl gave isosbestic behavior with ligands adding in one apparent step, *i.e.* $K_7 > K_6$. For this circumstance, plots of log([py]) vs $\log[(A - A_0)/(A_c - A)]$ have two distinct linear regions where the slope = 1, with an x-axis intercept = $-\log_1$, at low [py], and slope = 2, with an x-axis intercept at $-^1/_2 \log(\beta_2)$ for higher [py]. These relationships apply to cases where the UV absorption spectra for the initial five-coordinate complex and its base adduct are similar. The deviations shown in Figure 16, as well as in the spectra in Figure 14, indicate that the latter criteria do not apply for **1**. However, the first eight additions are linear, with slope = 1, and thus indicative that the first equilibrium corresponds to the addition of one pyridine. Deviations at higher pyridine concentrations are due to competition with the second reaction. The first equilibrium constant for pyridine association with **1** can be estimated by extrapolation as $K_6 = 20 \pm 6$.

(26) Polster, J.; Lachmann, H. *Spectrophotometric Titrations*; VCH: New York, 1989; Chapter 7, pp 67–132.
(27) Walker, F. A.; Lo, M.; Ree, M. T. *J. Am. Chem. Soc.* **1976**, *98*, 5552.

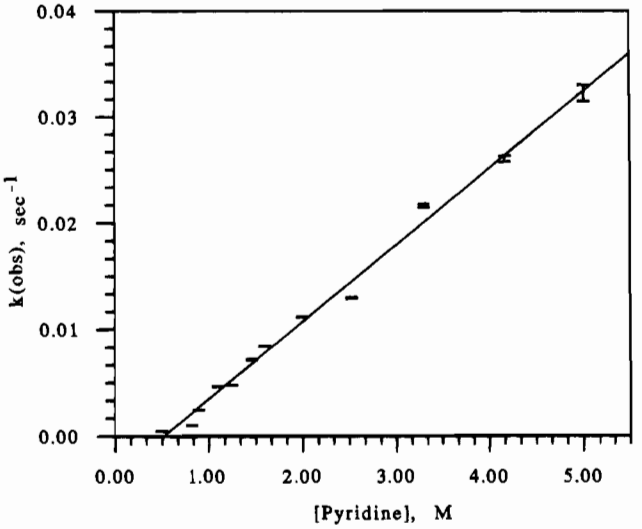

Figure 17. Dependence of k(obs) on pyridine concentration for the reaction shown in eq 8.

Table 8. Rate Constants (k(obs)) for Eq 8 at Different Pyridine Concentrations[a]

[py], M	10^2k(obs)	[py], M	10^2k(obs)
0.50	$(4.87 \pm 0.02) \times 10^{-2}$	1.60	$(8.43 \pm 0.02) \times 10^{-1}$
0.82	$(1.02 \pm 0.01) \times 10^{-1}$	2.00	1.12 ± 0.01
0.89	$(2.47 \pm 0.01) \times 10^{-1}$	2.53	1.30 ± 0.01
1.09	$(4.67 \pm 0.05) \times 10^{-1}$	3.30	2.16 ± 0.02
1.25	$(4.77 \pm 0.02) \times 10^{-1}$	4.17	2.60 ± 0.03
1.45	$(7.17 \pm 0.03) \times 10^{-1}$	5.01	3.22 ± 0.08

[a] Fe(TTP)[ONC(CN)$_2$] concentration: 1.00×10^{-4} M in toluene at 25 °C.

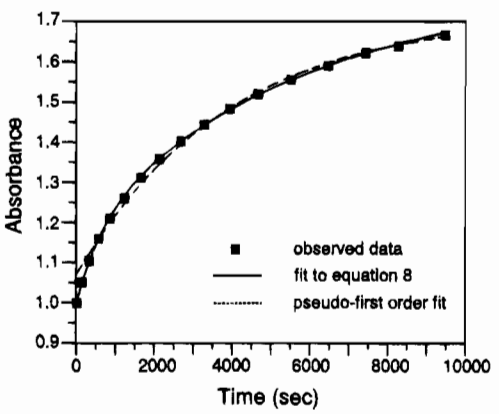

Figure 18. Predicted and observed absorbance changes for eq 8 with 0.3 M pyridine.

To help clarify some of the results observed during the spectrophotometric titrations, the kinetics for this process were observed under a range of pyridine concentrations. As is shown in Figure 17 and Table 8, at high concentrations of pyridine the rate is linearly dependent upon base concentration and the reaction exhibits pseudo-first-order kinetics. At low pyridine concentrations, 0.45 M and less, the observed absorption changes, Figure 18, deviate significantly from first order and have been fitted by principal factor analysis and Marquardt minimization[28] to a reversible preequilibrium second-order step followed by a first-order irreversible step to give the observed products, eq 8. For a pyridine concentration of 0.30 M, $k_1 = (6.5 \pm 0.3) \times 10^{-4}$ L M^{-1} s^{-1}, $k_{-1} = (1.4 \pm 0.5) \times 10^{-4}$ s^{-1},

(28) *SPECFIT: A Program for Global Least Squares Fitting of Equilibrium and Kinetic Systems Using Factor Analysis and Marquardt Minimization*; Spectrum Software Associates: Chapel Hill, NC, 1993.

$$Fe(TTP)\{ONC(CN)_2\} + py \underset{k_{-1}}{\overset{k_1}{\rightleftharpoons}} Fe(TTP)\{ONC(CN)_2\}(py) + py \xrightarrow{k_2} [Fe(TTP)(py)_2]^+ [ONC(CN)_2]^- \quad (8)$$

and $k_2 = (1.39 \pm 0.01) \times 10^{-3}$ s^{-1}. These results give a kinetically determined equilibrium constant, $K_6 = 5$, an order of magnitude less than that estimated by spectrophotometric titration. This reaction exhibits four isosbestic points, at 541, 512, 492, and 476 nm, and evolving factor analysis predicts that the intermediate will have Q-bands at 560 and 530 nm, values very similar to those for the final product, $[Fe(TTP)(py_2)]^+$.

Discussion

There is a surprising degree of similarity in the chemistries of the nitrite and nitrosodicyanomethanide anions. Both exhibit distinct solvatochromism with the λ_{max} blue-shifted in hydrgoen-bonding solvents. In water the nitrosodicyanomethanide bands at 406 and 266 nm are red-shifted *ca.* 50 nm compared to the corresponding bands in nitrite at 348 and 217 nm. Clearly the HOMO−LUMO gap in nitrosodicyanomethanide is smaller than that in nitrite, and this feature correlates with the observed strong π-accepting character for the N-bound isomer present in **2**. Furthermore, the calculated charge densities by a Mulliken population analysis, Table 7, indicate that the oxygen is slightly less charged, −0.49, vs the oxygens in nitrite, −0.59, for the optimized geometries calculated at the MP2 level of theory with a 6-311G* basis set. The observed and calculated O−N−C angles in the nitrosodicyanomethanide anion and its complexes are only slightly larger, <1°, than those found for related nitrite species. Finally, the oxidation potential of nitrous acid, for the couple HNO_2/N_2O_4, 1007 mV, is larger than the value for nitrosodicyanomethanide.

A consequence of these properties is that nitrosodicyanomethanide is a better π-acceptor as an N-bound ligand and a better σ-donor as an O-bound ligand than is nitrite. However, the nitrosodicyanomethanide ligand is subject to steric constraints that nitrite is not, namely the cyano substituent on the same side as the nitrogen lone pair. Although this steric effect is not a factor in the formation of the square planar complex **2** or an octahedral pentacarbonylrhenium(I) complex,[29] we suggest that one factor which favors the O-bound geometry in **1** would be the juxtaposition of the large porphyrin ring to the cyano substituents in nitrosodicyanomethanide. Conversely, the high charge density of the oxygen in nitrosodicyanomethanide will favor oxygen binding in very electrophilic centers such as in a high-spin iron(III) porphyrin center.[30]

Although both solution/glass ESR measurements and the solid state magnetic susceptibility results are consistent with **1** being formulated as a high-spin $S = {}^5/_2$ complex, the X-ray diffraction results are somewhat anomalous. The high-spin ferric porphyrins are characterized by iron to mean porphyrin plane separations between 0.5 and 0.4 Å, while the value observed in the structure of **1**, 0.359 Å, is close to the range usually attributed to intermediate-spin-state systems.[31] In addition to the out of plane separations, the iron−nitrogen bond lengths in **1** are significantly shorter than the range usually found in a five-coordinate high-spin complex, 2.060−2.087 Å.[31] These structural distinctions may be attributable to the formation of the I type π-stacked dimer pair in the solid state, but we note that both $S = {}^3/_2$ and $S = {}^5/_2$ ferric porphyrin complexes form I type dimers. Furthermore, the complex most crystallographically similar to **1** is $Fe(TPP)(B_{11}CH_{12})$, which is best described as being an admixture of $S = {}^3/_2$ (92%) and $S = {}^5/_2$ (8%).[30]

The kinetics and thermodynamics of pyridine addition to **1** are also somewhat anomalous and fall between the behaviors found for $Fe^{III}(Por)X$ where X = halide and X = cyanide, azide, or thiocyanate. In the former cases ligand substitution occurs rapidly at room temperature to give the bis(ligand) product. In the latter case the second addition is slow and in several cases is not favored at all. The product from the addition of base to the azido and cyano complexes are six-coordinate Fe(por)X(py) complexes.[32] The nitrosodicyanomethanide complex **1** falls between these two extremes, as the equilibrium constant for binding the first and the second pyridine ligands are not as disparate.[33] Moreover, the rate of the second pyridine addition is slightly faster than the first, unlike the addition of imidazole and *N*-methylimidazole to Fe(TPP)Cl, where there is a large difference in the rates for the two steps.

Scheidt has shown in a series of elegant studies that nitrite complexes of iron(III) porphyrins are low-spin six-coordinate species that are almost exclusively N-bound (nitro).[34] In general, these complexes undergo facile O atom transfer to mercaptide[34a] or tertiary phosphine[25] to give five-coordinate nitrosyl adducts of ferrous porphyrins after loss of the *trans* axial ligand.[35] In only one instance is there any evidence to propose the presence of O-bound nitrite, that is the nitrito complex $[Fe(TPP)(NO)(ONO)]^-$, in these studies.[34b] These trends are not limited to the porphyrin complexes of iron(III), and it is surprising how poorly developed the coordination chemistry of iron nitrites is in comparison with that of their cobalt and nickel analogs. Part of the interest in the iron porphyrin nitrite system stems from the presence of a catalytically active heme site in the nitrite reductases found in a variety of faculative anaerobic bacteria.[36] A range of spectroscopic studies, most notably EPR,[37] have identified a heme nitrosyl adduct as the initial one-electron-reduced species. While many studies have modeled aspects of this reductase activity,[38a−d] our knowledge of the ligand sphere coordination chemistry of nitrite in heme centers remains limited by their facile reduction to a nitrosyl complex and the stability of the N-bound geometry over O-bound isomer. The isolation of **1**, an analog of a O-bound nitrito complex, allows for aspects of the chemistry of the heterofore illusive nitrito complexes to be inferred.

(29) Fritsch, E.; Polborn, K.; Sünkel, K.; Beck, W.; Köhler, H.; Jäger, L. *Z. Anorg. Allg. Chem.* **1992**, *617*, 110.
(30) Gupta, G. P.; Lang, G.; Lee, Y. J.; Scheidt, W. R.; Shelly, K.; Reed, C. A. *Inorg. Chem.* **1987**, *26*, 3022.
(31) Scheidt, W. R.; Gouterman, M. In *Iron Porphyrins, Part I*; Lever, Gray, Eds.; Addison-Wesley: Reading, MA, 1983; p 89.
(32) (a) Scheidt, W. R.; Lee, Y. J.; Geiger, D. K.; Taylor, K.; Hatano, K. *J. Am. Chem. Soc.* **1982**, *104*, 3367. (b) Summerville, D. A.; Cohen, I. A.; Hatano, K.; Scheidt, W. R. *Inorg. Chem.* **1978**, *17*, 2906. (c) Scheidt, W. R.; Lee, Y. J.; Luangdilok, W.; Haller, K. J.; Anzai, K.; Hatano, K. *Inorg. Chem.* **1983**, *22*, 1516. (d) Adams, K. M.; Rasmussen, P. G.; Scheidt, W. R.; Hatano, K. *Inorg. Chem.* **1979**, *18*, 1892.
(33) Trondeau, G. A.; Sweigart, D. A. *Inorg. Chem.* **1984**, *23*, 1060.
(34) (a) Nasri, H.; Haller, K. J.; Wang, Y.; Huynh, B. H.; Scheidt, W. R. *Inorg. Chem.* **1992**, *31*, 3459. (b) Finnegan, M. G.; Lappin, A. G.; Scheidt, W. R. *Inorg. Chem.* **1990**, *29*, 181.
(35) Bonnett, R.; Charalambides, A. A.; Martin, R. A. *J. Chem. Soc., Perkin Trans. 1* **1978**, 974.
(36) Henry, Y.; Bessières, P. *Biochemie* **1984**, *66*, 259.
(37) Johnson, M. K.; Thomson, A. J.; Walsh, T. A.; Barber, D.; Greenwood, C. *Biochem. J.* **1980**, *189*, 285.
(38) (a) Barley, M. H.; Takeuchi, K. J.; Meyer, T. J. *J. Am. Chem. Soc.* **1986**, *108*, 5876. (b) Fernandes, J. B.; Feng, D.-W.; Chang, A.; Keyser, A.; Ryan, M. D. *Inorg. Chem.* **1986**, *25*, 2606. (c) Choi, I.-K.; Ryan, M. D. *Inorg. Chim. Acta* **1988**, *153*, 25. (d) Choi, I.-K.; Liu, Y.; Feng, D.-W.; Paeng, K.-J.; Ryan, M. D. *Inorg. Chem.* **1991**, *30*, 1832. (e) Settin, M. F.; Fanning, J. C. *Inorg. Chem.* **1988**, *27*, 1431.

Experimental Section

Materials. General experimental practices and instrumentation have described previously.[39] Silver nitrosodicyanomethanide was prepared by the method of Iglesias and Williams from malononitrile and nitrous acid in buffered acetic acid/sodium acetate followed by precipitation with silver ion.[11] The malononitrile used in the synthesis of silver nitrosodicyanomethanide was dried and sublimed before use. Otherwise all starting materials were obtained commercially and used without further purification. For inert-atmosphere operation solvents were dried, distilled, and degassed by standard techniques.[40]

Electrochemistry. All cyclic and square-wave voltammetric experiments were performed with a BAS-50W potentiostat in a Vacuum Atmospheres inert-atmosphere box. In each case the cell consisted of a platinum button working electrode, a platinum wire auxiliary electrode, and a $Ag/AgNO_3/CH_3CN$ reference electrode with 0.1 M tetra-*n*-butylammonium hexafluorophosphate as supporting electrolyte in either dichloromethane or acetonitrile. All reported potential values are referenced to the internal ferrocene/ferrocenium couple.

The spectroelectrochemistry experiments were performed in an OTTLE fabricated after the design of Paulson and Elliott.[41] In this cell platinum wire gauze is the working electrode which is sandwiched between quartz plates. The cell characteristics include a path length of 0.007 cm, electrode area of 0.20 cm^2, and a thin-layer volume of 0.0013 cm^3. The light beam illuminates about 0.1 cm^2 in the center of the electrode. The reference electrode is a silver wire and the auxiliary electrode is a platinum wire maintained within 0.5 cm of the working/electrode in the optical cell.

Electron Paramagnetic Resonance. EPR spectra were obtained on a Varian E-3 X-band spectrometer with a low-temperature cryostat. A sample of 0.01 M Fe(TTP)[ONC(CN)$_2$] in toluene was contained in a 4 mm quartz tube sealed under nitrogen in an inert-atmosphere box. The spectrum was obtained at 77 K in a toluene glass. The reported g values were referenced to DPPH (g = 2.002 32).

Magnetic Susceptibility. Magnetic susceptibility data was obtained either by the Faraday method on a Johnson Matthey magnetic susceptibility balance or with a Quantum Design MPMS5 5 T SQUID magnetometer. The Faraday balance was calibrated against $HgCo(SCN)_4$, $\chi_m = 7.92 \times 10^{-3}$ emu mol^{-1}. The diamagnetic corrections for **1** were determined on this balance by measuring the magnetic susceptibility of tetratolylporphyrin ($TTPH_2$) ($\chi_m = -7.71 \times 10^{-4}$ emu mol^{-1}) and Ag[ONC(CN)$_2$] ($\chi_m = -5.27 \times 10^{-5}$ emu mol^{-1}) and employing the literature value for the correction of Ag^+ ($\chi = -2.7 \times 10^{-5}$ emu mol^{-1}). The SQUID results were obtained on a 24.89 mg sample with a field of 5000 G.

Kinetics Studies. The dissociation rate constants of Fe(TTP)[ONC(CN)$_2$] with pyridine were measured by using a combined cell/flask/mixing chamber described by Basolo and Clarkson.[42] The reactions were followed by monitoring the absorbance change of the 530 nm wavelength by means of HP-8452A spectrophotometer equipped with a thermostated cell holder held at 25 °C. For the kinetic measurements with pyridine concentrations greater than 0.75 M, the concentrations of the metal complex were in the range of 1×10^{-4} M and the concentration of the pyridine was at least 100-fold in excess of the base over the metal concentration so the reactions were run under pseudo-first-order conditions with respect to the iron complex. Rate constants were obtained by plots of $\ln(A_t - A_\infty)$ vs time where A_t is the absorbance at time t and A_∞ is the absorbance at infinite reaction time. All of the plots show excellent linearity for at least 4 half-lives. For pyridine concentrations less than 0.75 M the wavelength range from 450 to 650 nm was measured and then fitted with the Specfit program using evolving factor analysis.[28] The thermodynamic equilibrium constants were determined by analysis of A plots constructed at several wavelengths from spectrophotometric titrations of **1** with pyridine.[26]

Theoretical Methods. Ab initio calculations were performed on a Silicon Graphics Crimson workstation with the Gaussian92 package.[43] Geometry optimizations were performed using Cartesian coordinates with gradient techniques. The full active MP2 space has been used. The frequencies calculated at the Møller–Plesset level 2 were obtained using the numerical direct SCF algorithm.

Preparation of New Compounds. Fe(TPP)[ONC(CN)$_2$], 1. To a solution of 0.409 g (0.54 mmol) of Fe(TTP)Cl[44] in 20 mL of benzene was added 0.118 g (0.59 mmol) of Ag[ONC(CN)$_2$]. The solution was stirred at room temperature for 15 min. The resulting silver chloride was removed by filtration, and the product was then precipitated by slowly adding hexane to the filtrate to give 0.363 g (82%). UV–vis, in toluene, λ_{max} (nm) (log $\epsilon(M^{-1}\ cm^{-1})$): 365 (4.61, sh), 414 (5.09), 512 (4.10), 574 (3.53), 660 (3.38, sh), 694 (3.49). Magnetic susceptibility: μ = 5.36 at 298 K. Anal. Calcd for $C_{51}H_{36}N_7OFe$: C, 74.80; H, 4.43; N, 11.98. Found: C, 74.67; H, 4.22; N, 11.66. A crystal suitable for single-crystal X-ray diffraction was grown from dichloromethane/hexanes by vapor phase diffusion.

Ir{η^1-N(O)C(CN)$_2$}(CO)(PPh$_3$)$_2$, 2. $IrCl(CO)(PPh_3)_2$, 49 mg (6.23×10^{-5} mol), and tetramethylammonium nitrosodicyanomethanide, **3** (3.1×10^{-4} mol, 5 equiv), were dissolved in 25 mL of 1:1 dichloromethane/ethanol, and the mixture was stirred for 15 min to give a bright yellow solution. Removal of the dichloromethane gave bright yellow crystals, which were further purified by recrystallization from dichloromethane/ethanol to give 44 mg (84%) of yellow prisms. Anal. Calcd for $C_{40}H_{30}O_2IrN_3$: C, 57.03; H, 3.60; N, 5.01. Found: C, 57.03; H, 3.52; N, 4.89. UV–vis, in dichloromethane, λ_{max} (log ϵ) = 438 nm (3.42). IR (Nujol), cm^{-1}: 2219.9 m, 2203.5 m {ν(CO)}; 1997.2 s, 1973.2 s {ν(CO)}; 1328.9 m, 1251.7 w, 803.3 w. IR (CH_2Cl_2), cm^{-1}: 2220.3 m, 2209.7 m {ν(CN)}; 1993.7 s {ν(CO)}. Crystals suitable for single-crystal X-ray diffraction were grown from dichloromethane/*n*-hexane by vapor phase diffusion.

[NMe$_4$][ONC(CN)$_2$] 3. Silver nitrosodicyanomethanide,[10] 1.34 g (6.6×10^{-3} mol), was suspended in 20 mL of dichloromethane and treated with tetramethylammonium chloride, 836 mg (7.6×10^{-3} mol, 1.15 equiv), as an acetonitrile solution. A dense white precipitate of silver chloride rapidly formed, and after 20 min of stirring, the yellow solution was separated from the mixture by filtration through Celite. The solution was concentrated to 2 mL on a rotorary evaporator, and the product was precipitated by the dropwise addition of ether. Recrystallization of this material from acetone/heptane gave 1.01 g (94% yield) of bright yellow needles: mp 184–5 °C. Anal. Calcd for $C_7H_{12}N_4O$: C, 50.24; H, 7.22; N, 33.03. Found: C, 49.99, H; 7.19; N, 33.31. ^1H NMR (CD_3CN), δ: 3.09 (s, N(CH_3)$_4$). $^{13}C\{^1H\}$ NMR, δ: 56.26 (s, N(CH_3)$_4$); 114.00, 120.14 (s, *C*N); 108.20 (s, ON*C*). IR (KBr), cm^{-1}: ν(CN) 2212.2 s, 2203.9 s; $\nu(CNO)_a$ 1296 sh, 1279.1 m; $\nu(CNO)_s$ 1237.7 m; other bands at 1487.4 s, 950.3 m, 780.6 m, 579.5 m. UV–vis, λ_{max} (nm) (log $\epsilon(M^{-1}\ cm^{-1})$) [solvent]: 478 (159) [acetone]; 472 (130) [acetonitrile]; 428 (95), 298 (7800) [ethanol]; 406 (93), 266 (11 200) [water].

X-ray Data Collection and Structure Determination. Single-crystal X-ray data were collected on a Siemens R3m/V diffractometer equipped with a molybdenum tube [$\lambda(K\alpha_1)$ = 0.709 26 Å; $\lambda(K\alpha_2)$ = 0.713 54 Å] and a graphite monochromator. Throughout each data collection, three standard reflections were measured after every 100 reflections collected. In each case, the data were corrected for absorption using semiempirical techniques. Structure solution programs used were from the SHELXTL system. The structures were solved by Patterson techniques and refined by full-matrix least-squares techniques. Important crystal data for these structures are collected in Table 9.

(39) Bohle, D. S.; Carron, K. T.; Christensen, A. N.; Goodson, P. A.; Powell, A. K. *Organometallics* **1994**, *13*, 1355.
(40) Perrin, D. D.; Armarego, W. L. F. *Purification of Laboratory Chemicals*, 3rd ed.; Pergamon Press: Oxford, U.K., 1988.
(41) Paulson, S. C.; Elliott, C. M. *Anal. Chem.*, in press.
(42) Clarkson, S. G.; Basolo, F. *Inorg. Chem.* **1973**, *12*, 1528.
(43) Frisch, M. J.; Trucks, G. W.; Head-Gordon, M.; Gill, P. M. W.; Wong, M. W.; Foresman, J. B.; Johnson, B. G.; Schlegel, H. B.; Robb, M. A.; Replogle, E. S.; Gomperts, R.; Andres, K.; Raghavachari, K.; Binkley, J. S.; Gonzales, C.; Martin, R. L.; Fox, D. J.; DeFrees, D. J.; Baker, J.; Stewart, J. J. P.; Pople, J. A. *GAUSSIAN 92*; Gaussian Inc.: Pittsburgh, PA, 1992.
(44) Adler, A. D.; Longo, F. R.; Kampas, F.; Kim, J. *J. Inorg. Nucl. Chem.* **1970**, *2*, 2443.
(45) Zub, Y. L.; Sadikov, G. G.; Skopenko, V. V.; Porai-Koshits, M. A.; Nikolaev, V. P. *Koord. Khim.* **1985**, *11*, 532.
(46) Sadikov, G. G.; Zub, Y. L.; Skopenko, V. V.; Nikolaev, V. P.; Porai-Koshits, M. A. *Koord. Khim.* **1984**, *10*, 1253.
(47) Skopenko, V. V.; Zub, Y. L.; Porai-Koshits, M. A.; Sadikov, G. G. *Ukr. Khim. Zh.* **1979**, *45*, 811.
(48) Chow, Y. M.; Britton, D. *Acta Crystallogr.* **1974**, *B30*, 1117.

Table 9. Crystallographic Data

	1	2
formula	$C_{51}H_{36}FeN_7O$	$C_{40}H_{30}IrN_3O_2P_2$
a (Å)	11.725(2)	12.662(3)
b (Å)	13.851(3)	13.896(3)
c (Å)	14.382(3)	21.879(4)
α (deg)	108.74(3)	74.69(3)
β (deg)	95.07(3)	78.65(3)
γ (deg)	108.19(3)	83.10(3)
V (Å^3)	2054.6(7)	3630.9(13)
Z	2	4
fw	818.7	838.8
space group	$P\bar{1}$	$P\bar{1}$
T (°C)	23	23
λ (Å)	0.710 73	0.710 73
ϱ_{calc} (g cm^{-3})	1.323	1.534
μ(Mo Kα_1) (mm^{-1})	0.416	3.803
R^a	0.054	0.058
$R_w{}^a$	0.059	0.068

^{a} $R = \Sigma||F_o| - |F_c||/\Sigma|F_o|$; $R_w = [\Sigma w(|F_o| - |F_c|)^2/\Sigma w|F_o|^2]^{1/2}$.

Fe(TTP)[ONC(CN)$_2$], 1. Data were collected at 23 °C on a crystal of dimensions 0.87 × 0.18 × 0.26 mm. The compound crystallized in the centrosymmetric triclinic space group $P\bar{1}$, with two molecules in a cell of dimensions a = 11.725(2) Å, b = 13.851(3) Å, c = 14.382(3) Å, α = 108.74(3)°, β = 95.07(3)°, γ = 108.19(3)°, and V = 2054.6(7) Å^3. A total of 7220 independent reflections were gathered (R_{int} = 0.022), the octants collected being $+h,\pm k,\pm l$ using the Wyckoff scan method. The structure was refined to conventional R factor values of R = 0.0542 and R_w = 0.0587 on the basis of 4412 observed reflections with $I > 6\sigma(I)$ in the 2θ range 4−50°, giving a data to parameter ratio of 8.1:1. All non-hydrogen atoms were refined anisotropically, while the hydrogen atoms, located in the Fourier map, were refined isotropically. The maximum and minimum residual densities remaining were 0.40 and −0.29 e Å^{-3}, respectively. Selected metrical data and atomic positions are presented in Tables 1 and 2, and complete crystallographic details are collected in supplementary Tables S1−S5.

Ir{η^1-N(O)C(CN)$_2$}(CO)(PPh$_3$)$_2$, 2. Data were collected at 23 °C on a yellow prism of dimensions 0.03 × 0.12 × 0.09 mm. The compound crystallized in the centrosymmetric triclinic space group $P\bar{1}$, with four molecules in a cell of dimensions a = 12.662(3) Å, b = 13.896(3) Å, c = 21.879(4) Å, α = 74.69(3)°, β = 78.65(3)°, γ = 83.10(3)°, and V = 3630.9(13) Å^3 with ϱ(calcd) = 2.867 g mL^{-1}. A total of 13 677 independent reflections were gathered (R_{int} = 0.031), the octants collected being $+h,\pm k,\pm l$ using the ω-scan method. The structure has been refined to conventional R factor values of R = 0.0577 and R_w = 0.0676 on the basis of 7403 observed reflections with $I > 4\sigma(I)$ in the 2θ range 4−50°, giving a data to parameter ratio of 14.7:1. Except for the triphenylphosphine carbons, all non-hydrogen atoms were refined anisotropically. The hydrogen atoms were placed in fixed calculated positions (C−H = 0.96 Å). Absorption corrections based on the empirical ϕ scans were applied with maximum and minimum transmission coefficients being 0.986 and 0.601, respectively, and the linear absorption coefficient, μ, being 3.80 mm^{-1}. The maximum and minimum residual densities remaining were 1.09 and −1.27 e Å^{-3}, respectively. Selected metrical data and atomic positions are presented in Tables 3 and 4, and complete crystallographic details are given in supplementary Tables S6−S11.

Acknowledgment. We thank the Research Corp. for a Cottrell Scholar award to D.S.B. and the Arthritis Foundation and the American Heart Association, both the National Chapter and the Wyoming Affiliate, for their generous support of this research. We also acknowledge Professor Gordon T. Yee for helpful discussions and the National Institute of Standards and Technology for use of the SQUID magnetometer.

Supplementary Material Available: Tables giving summaries of the X-ray crystallographic results, positional and thermal parameters, and bond distances and angles for **1** and **2** and calculated geometries for [ONC(CN)$_2$]$^-$ (19 pages). Ordering information is given on any current masthead page.

IC941182Z